

## THE EFFECT OF REACTOR HEIGHT ON COAL GASIFICATION

by

**Cem DOLU and Lutfullah KUDDUSI**

Mechanical Engineering Department, Faculty of Mechanical Engineering,  
Istanbul Technical University, Istanbul, Turkey

Original scientific paper

<https://doi.org/10.2298/TSCI150526112D>

*A comprehensive 2-D numerical model has been developed to simulate the coal gasification and investigate the effect of reactor height on the coal gasification in fluidized bed. Gas-solid flow, homogeneous and heterogeneous chemical reactions were considered. An Eulerian model for fluid phase and discrete particle method (Lagrangian) for particle phase were used in this study. The reaction rates of homogeneous and heterogeneous reactions were determined by Arrhenius-eddy dissipation reaction rate and Arrhenius-diffusion rate, respectively. Simulations were performed in a fluidized bed coal gasifier with twelve different reactor heights and with a diameter of 0.22 m. The calculated values were compared with the experimental values for the reactor height of 2 m available in open literature. It shows that the predicted exit gas mole fractions are in a good agreement with the experimental data.*

Key words: coal gasification, Eulerian-Lagrangian model, fluidized bed, simulation, reactor height effect\*

### Introduction

Gasification aim is to produce synthetic gas (syngas) which is primarily a mixture of H<sub>2</sub> and CO as fuels. An incomplete combustion process is mainly critical requirement for gasification. In other words, gasification is an incomplete combustion process which occurs with restricted oxygen. Variety of carbon-based feedstocks can be used for gasification process, such as coal, heavy refinery residues, petroleum coke, biomass, and miscellaneous carbon based wastes. The syngas can be utilized as fuel ordinarily for boilers or gas turbine to generate electricity. Coal gasification modeling is progressively prevalent with researchers to aid with design, investigation and optimization of coal gasification processes. The CFD model has got preferences by coupling the detailed fluidized bed hydrodynamics and reaction kinetics. Numerical simulations have got to be mainstream because of experimental adversities for coal gasification. The CFD modeling has a significant benefit to adequately overcome all hardships between large scale commercialized beds and small scale experimental set-ups.

There are two approaches for modeling multiphase flow, especially gas-solids flow system: Eulerian-Eulerian (E-E) model and Eulerian-Lagrangian (E-L) model. Solid phase is behaving towards as a continuum in E-E model and Eulerian groundwork is applied to describe the motion of solids [1]. In other words, the gas and solid phases are treated as interpenetrating continuum present at the same time in the same control volume. The conservation of mass and momentum equations are utilized for each phase and represented by respective conservation

\*Corresponding author, e-mail: doluce@itu.edu.tr

equations. The interaction between two phases is indicated as additional source terms that are added to the conservation equations. The conservation equations for mass and momentum are resolved for the gas and solid phase independently and closed with suitable constitutive relations. The E-E model got to be more mainstream after the advancement of kinetic theory of granular flow (KTGF) which is taking into account the theory of non-uniform dense gases depicted in [2]. This model has been efficiently used to forecast and validate lots of multi flow phenomena in gas-solid system such as the work of Wachem *et al.* [3] that utilized the model by taking into account two fluid models including the KTGF to simulate the bubble behavior in fluidized beds and compared the results with experimental data. Benyahia *et al.* [4] and Zhong *et al.* [5] likewise individually utilized KTGF to study the dense gas-solid flow characteristic in fluidized bed and spout-fluid bed. In the E-L model, the gas phase is treated as a continuum and time averaged Navier-Stokes equations are solved for gas phase while the solid phase is solved by tracking each and individual particle in Lagrangian frame. Mass, momentum, and energy transfer happen between the gas and solid phase. The E-L model is more costly about computational time compared to the E-E model. Particularly computational time is extremely influenced by the number of particles in the E-L model [6]. Discrete particle model (DPM) is generally applied to the particle description in the E-L model. This method can create elaborated information about solid phase such as trajectories of particles [7]. Grabner *et al.* [8] used the E-L model at circulating fluidized bed conditions however, they did not take particle collisions into account.

The current work is related to 2-D numerical steady-state model for fluidized bed coal gasification with using E-L DPM method. The ANSYS Fluent 13 is used for modeling and, homogeneous and heterogeneous reactions are considered. Model results are validated with experimental data [9]. After model validation, reactor height effect on CO and H<sub>2</sub> mole fractions is investigated.

### Numerical model

The E-L DPM method is embraced to tackle coal gasification modeling and numerical model is 2-D steady-state model in this study. Segregated solution strategy is utilized in solving the governing equations. The non-linear governing equations are implicitly linearized. The governing equations are discretized spatially to yield discrete algebraic equations for each volume. The second order scheme is used as the discretization scheme. The SIMPLE algorithm is utilized to couple the pressure and velocity. The fluid dynamics is depicted by averaged Navier-Stokes equations with strong coupling with the particle phase. The particle momentum equation follows the multi-phase-particle-in-cell formulation [10].

### Governing equations

Mass, momentum, and energy of the two-phase mixture are preserved by exchange terms in the fluid phase, respectively, mass, momentum, and energy equations. Species transport equations are figured out for all gas species included. The gas phase is modeled with a standard  $k$ - $\epsilon$  model on Eulerian grid. The particle phase is represented with discrete particle. The P-1 model is utilized as the radiation model. Stochastic tracking schemes are disposed to model the impacts of turbulence on the particles. The continuous phase and discrete phase are communicating each other with drag forces, lift forces, heat transfer, mass transfer, and species transfer. The time averaged, steady-state Navier-Stokes equations are tackled. The conservation of mass, momentum, and energy equations are given, respectively:

$$\frac{\partial(\rho u_i)}{\partial x_i} = S_m \quad (1)$$

$$\frac{\partial(\rho u_i u_j)}{\partial x_i} = \rho g_j - \frac{\partial P}{\partial x_j} + \frac{\partial(\tau_{ij} - \overline{\rho u_i u_j})}{\partial x_i} + S_f \quad (2)$$

$$\frac{\partial(\rho c_p u_i T)}{\partial x_i} = \frac{\partial}{\partial x_i} \left( \lambda \frac{\partial T}{\partial x_i} - \rho c_p \overline{u_i T'} \right) + \mu \Phi + S_h \quad (3)$$

where  $S_m$  is the mass source and  $S_f$  and  $S_h$  are the momentum and energy source terms, respectively. Besides, the source term  $S_h$  includes energies both from particles and radiation. The  $\Phi$  is the viscous dissipation. The symmetric stress tensor,  $\tau_{ij}$  is given:

$$\tau_{ij} = \mu \left( \frac{\partial u_j}{\partial x_i} + \frac{\partial u_i}{\partial x_j} - \frac{2}{3} \delta_{ij} \frac{\partial u_k}{\partial x_k} \right) \quad (4)$$

The species transport model is utilized to model the mixing and transport of the chemical species. The mathematical statement for species transport is:

$$\frac{\partial(\rho u_i C_j)}{\partial x_i} = \frac{\partial}{\partial x_i} (\overline{\rho u_i C_j}) + S_j \quad (5)$$

where  $S_j$  is the source term to accept increased or decreased chemical species resulted from chemical reactions. The standard  $k$ - $\varepsilon$  turbulence model is took into account in this study. Reynolds stresses are identified in the standard  $k$ - $\varepsilon$  model:

$$-\overline{\rho u_i u_j} = \mu_t \left( \frac{\partial u_i}{\partial x_j} + \frac{\partial u_j}{\partial x_i} \right) - \frac{2}{3} \rho k \delta_{ij} \quad (6)$$

where  $k$  is the turbulence kinetic energy and  $\mu_t$  is the turbulence viscosity that is given by:

$$\mu_t = \frac{\rho C_\mu k^2}{\varepsilon} \quad (7)$$

where  $C_\mu$  is a constant and  $\varepsilon$  is the turbulence dissipation rate. The equations for the turbulence kinetic energy ( $k$ ) and dissipation rate ( $\varepsilon$ ) are:

$$\frac{\partial(\rho u_i k)}{\partial x_i} = \frac{\partial}{\partial x_i} \left[ \left( \mu + \frac{\mu_t}{\sigma_k} \right) \frac{\partial k}{\partial x_i} \right] + G_k - \rho \varepsilon \quad (8)$$

$$\frac{\partial(\rho u_i \varepsilon)}{\partial x_i} = \frac{\partial}{\partial x_i} \left[ \left( \mu + \frac{\mu_t}{\sigma_\varepsilon} \right) \frac{\partial \varepsilon}{\partial x_i} \right] + C_{1\varepsilon} G_k \frac{\varepsilon}{k} - C_{2\varepsilon} G_k \rho \frac{\varepsilon^2}{k} \quad (9)$$

where  $G_k$  is the generation of turbulence kinetic energy because of the mean velocity gradients. The turbulent heat flux and mass flux can be modeled with the turbulent heat conductivity ( $\lambda_t$ ) and the turbulent diffusion coefficient ( $D_t$ ), respectively.

$$\overline{\rho c_p u_i T'} = -\lambda_i \frac{\partial T}{\partial x_i} = -c_p \frac{\mu_i}{Pr_i} \frac{\partial T}{\partial x_i} \quad (10)$$

$$\overline{\rho u_i C'} = -\rho D_i \frac{\partial C}{\partial x_i} = -\frac{\mu_i}{Sc_i} \frac{\partial C}{\partial x_i} \quad (11)$$

The constants  $C_{1\varepsilon}$ ,  $C_{2\varepsilon}$ ,  $C_\mu$ ,  $\sigma_k$ , and  $\sigma_\varepsilon$  values are used as: 1.44, 1.92, 0.09, 1 and 1.3, respectively [11].

### Radiation model

The P-1 radiation model is the least difficult one in the P-N model family, which is in view of the expansion of the radiation intensity into orthogonal series of spherical harmonics. The P-1 method is suitable for the heat radiation in the diffuse and optically thick media. The P-1 model can be depicted by a transport equation for radiation, temperature, which is a conservative equation and can be effortlessly consolidated into a CFD code. The P-1 model requires comparatively little request and can smoothly be applied to various entangled geometries. It is suitable for applications where the optical thickness  $a \times L$  is large; where  $a$  is the absorption coefficient and  $L$  is the length scale of the domain. In a gasifier, the optical thickness is thick because of the presence of various gases, coal particles, soot, and ashes. There are few restrictions for this model. First, the P-1 model supposes all surfaces are diffuse, which means the reflection of incident radiation at the surface is isotropic with respect to the solid angle. Second, the application of the P-1 model expects gray radiation. Third, when optical thickness is small, the P-1 model may lose some precision, depending upon the complexity of the geometry. Meanwhile, the P-1 model has a tendency to over predict the radiative flux from localized heat sources or sinks. The heat sources or sinks due to radiation are calculated by using the following equation:

$$-\nabla q_r = aG - 4aG\sigma a^4 \quad (12)$$

where  $G$  is the incident radiation,  $\sigma$  – the Stefan-Boltzmann constant, and  $q_r$  – the radiation heat flux and its equation is given:

$$q_r = \frac{-\nabla G}{3(a + \sigma_s) - C\sigma_s} \quad (13)$$

where  $\sigma_s$  is the scattering coefficient, and  $C$  – the linear-anisotropic phase function coefficient. The gases are assumed to be the participating media. However, when the effect of particles is included in the radiation model, the heat sources or sinks due to radiation become:

$$-\nabla q_r = -4\pi \left( \frac{a\sigma T^4}{\pi} + \varepsilon_p \right) + (a + a_p) \nabla G \quad (14)$$

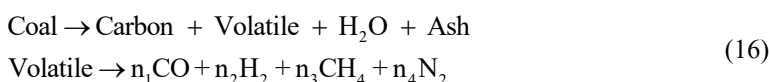
where  $\varepsilon_p$  and  $a_p$  are the equivalent emissivity and equivalent absorption of the particle, respectively. The flux of the radiation,  $q_{r,w}$  at walls caused by incident radiation  $G_w$  is given:

$$q_{r,w} = -\frac{4\pi\varepsilon_w \frac{\sigma T_w^4}{\pi} - (1 - \rho_w) G_w}{2(1 + \rho_w)} \quad (15)$$

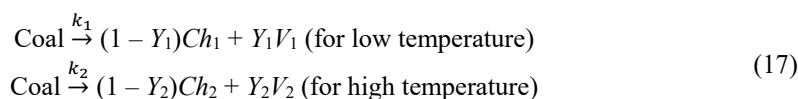
where  $\rho_w$  is the wall reflectivity,  $T_w$  – the surface temperature of the wall, and  $\varepsilon_w$  – the wall emissivity.

### Devolatilization model

Three main chemical processes have critical significance in coal gasification: coal devolatilization, heterogeneous char reactions, and homogeneous reactions of gas phase. Coal pyrolysis and composition balance of coal are taken into account:



The volatile matters comprised in the coal are assumed to be constituted by CO, H<sub>2</sub>, CH<sub>4</sub>, and N<sub>2</sub> [12]. In this study, all of the volatile matters are lumped into one volatile gas species. The devolatilization is assumed to start when the particle is heated up to 500 K. The volatile gas species is C<sub>1.08</sub>H<sub>3.68</sub>O<sub>0.67</sub>N<sub>0.18</sub> and it is calculated from the coals ultimate and approximate analysis [13]. Once volatile is released, it is decomposed into the CO, H<sub>2</sub>, CH<sub>4</sub> and N<sub>2</sub> gases through chemical reaction that is given as reaction 1 (R1) in tab. 1. In the current model, reactions with sulfur are ignored for their little amount. Coal particle has got moisture and the coal particle undergoes devolatilization after all the moisture contained in the coal particle has evaporated. Models for coal devolatilization have been developed and several reviews of these models have been published [14, 15]. In the present work, the well known two-step method for coal devolatilization is used and it is given:



where  $Ch_{1(2)}$  is the char which has not reacted,  $Y_{1(2)}$  is volatilization coefficient ( $Y_1 = 0.3$  and  $Y_2 = 1.0$ ), and  $V_{1(2)}$  is the volatile. Besides,  $k_1$  and  $k_2$  are the rate constant with Arrhenius form and these kinetic rate constants that may control the devolatilization over different temperature ranges are given by:

$$k_1 = A_1 \exp(-E_1 / RT_p) \quad (18)$$

$$k_2 = A_2 \exp(-E_2 / RT_p) \quad (19)$$

The value of the constants are  $A_1 = 2 \cdot 10^5$ ,  $A_2 = 1.3 \cdot 10^7$ ,  $E_1 = 1.046 \cdot 10^8$  J/kmol, and  $E_2 = 1.67 \cdot 10^8$  J/kmol.

### Reaction models

The particle reaction model assumes that coal consists of volatiles, char, moisture, and ash. The coal gasification model proposed in this simulation consists of devolatilization, volatiles combustion, char combustion, and gasification.

#### *Homogeneous (gas phase) reactions*

Two approaches are adopted to solve homogeneous gas-phase reaction: eddy-dissipation model and finite-rate kinetic model. In this study, the finite-rate and eddy-dissipation models are both considered to compute the reaction rates. The smaller reaction rate calculated by finite-rate and eddy-dissipation is used. The eddy-dissipation model considers the turbulent mixing of the gases [16]. The eddy-dissipation model expects that the chemical reaction is faster than the time scale of the turbulent mixing of the species. The reaction is supposed to happen

instantaneously when the reactants meet. The net rate of production of species  $i$  due to reaction  $R_{i,r}$  is given by the smaller of the two expressions:

$$R_{i,r} = v'_{i,r} M_{w,i} A \rho \frac{\varepsilon}{k} \min R \left( \frac{Y_R}{v'_{R,r} M_{w,R}} \right) \quad (20)$$

$$R_{i,r} = v'_{i,r} M_{w,i} A B \rho \frac{\varepsilon}{k} \left( \frac{\sum_P Y_P}{\sum_j v''_{j,r} M_{w,j}} \right) \quad (21)$$

where  $v'_{i,r}$  is the stoichiometric coefficient of the reactant  $i$  in reaction  $r$ ,  $v''_{j,r}$  – the stoichiometric coefficient of the product  $j$  in reaction  $r$ ,  $Y_P$  – the mass fraction of any product species  $P$ ,  $Y_R$  – the mass fraction of a particular reactant  $R$ ,  $A$  – the empirical constant equal to 4.0, and  $B$  – the another empirical constant equal to 0.5. The smaller of the two expressions is utilized because it is the limiting value that determines the reaction rate.

The finite-rate kinetic model computes the reaction rate using a statement that considers temperature, and does not take into account the turbulent mixing of the species. For non-reversible reaction, the net source of chemical species  $i$  because of reaction is calculated as the sum of the Arrhenius reaction sources over  $N_R$  reactions that the species participate in:

$$R_i = M_{w,i} \sum_{r=1}^{N_R} \Gamma (v''_{i,r} - v'_{i,r}) \left( k_{f,r} \prod_{j=1}^N [C_{j,r}]^{(\eta'_{j,r} + \eta''_{j,r})} \right) \quad (22)$$

where  $M_{w,i}$  [kg kmole<sup>-1</sup>] is the molecular weight of species  $i$ ,  $v'_{i,r}$  – the stoichiometric coefficient of reactant  $i$  in reaction  $r$ ,  $v''_{i,r}$  – the stoichiometric coefficient of product  $i$  in reaction  $r$ ,  $k_{f,r}$  – the forward kinetic reaction rate constant for reaction  $r$  [s<sup>-1</sup>],  $C_{j,r}$  [kmole m<sup>-3</sup>] molar concentration of species  $j$  in reaction  $r$ ,  $\eta'_{j,r}$  – the rate exponent of reactant species  $j$  in reaction  $r$ , and  $\eta''_{j,r}$  – the rate exponent of product species  $j$  in reaction  $r$ . Reaction rate contents in Arrhenius form for all of the gas phase reactions (homogeneous reactions) are given in tab. 1.

**Table 1. Homogeneous reaction rate constants**

Homogenous reactions	Rate constants $k = AT^n \exp(-E/RT)$ ( $n = 0$ )	Ref.
R1: volatile $\rightarrow$ 0.67CO + 1.635H <sub>2</sub> + 0.41CH <sub>4</sub> + 0.08N <sub>2</sub> (Volatile decomposition)	Eddy disipation	
R6: CH <sub>4</sub> + O <sub>2</sub> $\rightarrow$ CO + H <sub>2</sub> (Volatiles gasification via CH <sub>4</sub> )	$A = 4.4 \cdot 10^{11}$ kg/Pa <sup>0.5</sup> sm <sup>2</sup> $E = 1.25 \cdot 10^8$ J/kmol	[17]
R7: CO + 1/2O <sub>2</sub> $\rightarrow$ CO <sub>2</sub> (Combustion)	$A = 2.2 \cdot 10^{12}$ kg/Pa <sup>0.5</sup> sm <sup>2</sup> $E = 1.67 \cdot 10^8$ J/kmol	[18]
R8: H <sub>2</sub> + 1/2O <sub>2</sub> $\rightarrow$ H <sub>2</sub> O (Oxidation)	$A = 2.5 \cdot 10^{16}$ kg/Pa <sup>0.5</sup> sm <sup>2</sup> $E = 1.68 \cdot 10^8$ J/kmol	[17]
R9: CO + H <sub>2</sub> O $\rightarrow$ CO + H <sub>2</sub> (Water gas shift)	$A = 2.75 \cdot 10^{10}$ kg/Pa <sup>0.5</sup> sm <sup>2</sup> $E = 8.38 \cdot 10^7$ J/kmol	[17]
R10: CO <sub>2</sub> + H <sub>2</sub> $\rightarrow$ CO + H <sub>2</sub> O (Backward water gas shift)	$A = 0.0265$ kg/Pa <sup>0.5</sup> sm <sup>2</sup> $E = 3960$ J/kmol	[17]

### Heterogeneous (solid-gas) reactions

Char is the residue part of the coal particle after the devolatilization process. The coal particle reactions occur after the devolatilization process has finished. Heterogeneous reactions of char with the gas species are a complex process which involves the balancing rate of mass diffusion of the oxidizing chemical species to the surface of a fuel particle with the surface reaction of these species with the char. The rate of depletion of solid (coal particle) due to surface reaction is expressed as a function of the kinetic rate. The reaction rates are global net rates. In this study, the commonly simplified heterogeneous reactions are used and the rate expressions and kinetic parameters for heterogeneous reaction rate constants are summarized in tab. 2.

**Table 2. Heterogeneous reaction rate constants**

Heterogenous reactions	Rate constants $k = AT^n \exp(-E/RT)$ ( $n = 0$ )	Ref.
R2: $C(s) + 1/2O_2 \rightarrow CO$ (Combustion)	$A = 0.052 \text{ kg/Pa}^{0.5}\text{sm}^2$ $E = 6.1 \cdot 10^7 \text{ J/kmol}$	[19]
R3: $C(s) + H_2O(g) \rightarrow CO + H_2$ (Gasification, boudouard reaction)	$A = 0.0782 \text{ kg/Pa}^{0.5}\text{sm}^2$ $E = 1.15 \cdot 10^8 \text{ J/kmol}$	[19]
R4: $C(s) + CO_2 \rightarrow 2CO$ (Gasification)	$A = 0.0732 \text{ kg/Pa}^{0.5}\text{sm}^2$ $E = 1.125 \cdot 10^8 \text{ J/kmol}$	[19]
R5: $C(s) + 2H_2 \rightarrow CH_4$ (Methanation reaction)	$A = 6 \cdot 10^{-7} \text{ kg/Pa}^{0.5}\text{sm}^2$ $E = 7.53 \cdot 10^7 \text{ J/kmol}$	[20]

The reaction of particle occurs after the devolatilization process has finished. The rate of depletion of solid due to a surface reaction is expressed:

$$\bar{R} = A_p \eta Y R \quad (23)$$

$$R = k \left( p_n - \frac{R}{D} \right)^N \quad (24)$$

where  $\bar{R}$  [ $\text{kg s}^{-1}$ ] is the rate of particle surface species depletion,  $A_p$  [ $\text{m}^2$ ] – the particle surface area,  $Y$  – mass fraction of surface the solid species in the particle,  $\eta$  – effectiveness factor,  $R$  [ $\text{kg m}^{-2}\text{s}^{-1}$ ] – rate of particle surface species reaction per unit area,  $p_n$  [Pa] – bulk partial pressure of the gas phase species,  $k$  – the kinetic reaction rate constant,  $N$  – apparent order of reaction, and  $D$  is diffusion rate coefficient for reaction that is given by

$$D = C_1 \frac{\left[ \frac{T_p + T_\infty}{2} \right]^{0.75}}{d_p} \quad (25)$$

where  $C_1$  is the mass diffusion limited rate constant ( $C_1 = 5 \cdot 10^{-12} \text{ m}^3/\text{K}^{0.75}\text{s}$ ) [15]. Apparent order of reaction can be taken 1 or 0 in FLUENT and  $N$  is taken 1 due to diffusion effect in the model. Besides, the effectiveness factor  $\eta$  is set unity (*i. e.*, not being used) for reaction rate model.

In this study, the finite-rate model is utilized for the heterogeneous reactions. Both the finite-rate and eddy-dissipation models are considered for the homogeneous reaction and the smaller of the two is used as the reaction rate. The finite-rate model calculates the reaction rates in view of the kinetics, while the eddy-dissipation model calculates based on the turbulent mixing rate of the flow.

### Numerical model boundary conditions and validation with experimental result

For the purpose of validating, all the operating and boundary conditions in this study are the same as those in the work of Chejne and Hernandez [9]. A schematic diagram of this

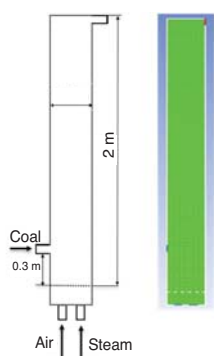


**Figure 1. Schematics of the reactor and simulation grid**

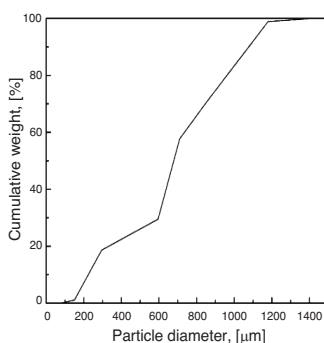


**Figure 2. Particle size distribution**

reactor and numerical simulation grids are presented in fig. 1. The diameter of the reactor is 22 cm and the reactor height is 200 cm. Air and steam inlets are at the bottom of the reactor. The coal feeder spotted at 30 cm above the distributor. The mean particle size is 0.62 mm and the size distribution is demonstrated in fig. 2. The air and steam stream into the distributor plate with 48 holes.

The outlet pressure is fixed to the atmosphere. The modeling conditions, for example, coal properties are given in tab. 3 and operating conditions and experimental results as indicated by the Chejne and Hernandez [9] experiment are given in tab. 4. These six different experimental results are used to verify numerical study.

**Table 3. Coal analyses and properties [9]**

Proximate analysis	Weight [%]
Moisture	2.6
Volatile matter	41.8
Fixed carbon	54.1
Ash	1.5
Ultimate analysis	Weight [%]
Carbon	75.3
Hydrogen	5.4
Nitrogen	1.8
Oxygen	15.6
Sulphur	0.4
Ash	1.5
Others	
High heating value [kJ <sup>-1</sup> kg]	29695
Mean particle diameter [mm]	0.62
Apparent density [kgm <sup>-3</sup> ]	1250

All mathematical models depicted above are executed in 2-D Cartesian co-ordinate framework by utilizing a finite volume method. A first-order upwind discretization is used for all solutions. To achieve a stable converged solution gas-solid flow without chemical reactions are solved first. After the essential flow pattern is secured chemical reactions are included. Converged results are attained when the residuals fulfill mass residual of  $10^{-3}$ , energy residual of  $10^{-5}$ , momentum and turbulence kinetic energy residuals of  $10^{-4}$ . These residuals are the summation of the imbalance in each cell. Figure 3 shows a graph of typical variable residuals.

**Table 4. Operating conditions and experimental results [9]**

Operating conditions	Exp. 1	Exp. 2	Exp. 3	Exp. 4	Exp. 5	Exp. 6
Coal feed [kg/h]	8.0	8.0	8.0	6.6	8.0	8.0
Air supply [kg/h]	19.4	21.9	17.0	14.8	21.9	28.4
Steam supply [kg/h]	4.6	4.6	4.6	4.0	4.6	4.6
Inlet temperature of air and steam [K]	695	693	686	609	708	641
Temperature of reactor [K]	1114	1128	1085	1102	1139	1099
Experimental results	Exp. 1	Exp. 2	Exp. 3	Exp. 4	Exp. 5	Exp. 6
H <sub>2</sub> (% mole fraction)	9.63	8.53	8.84	10.80	7.88	6.48
CO <sub>2</sub> (% mole fraction)	14.40	19.31	18.38	21.59	15.60	14.86
N <sub>2</sub> (% mole fraction)	64.62	60.38	61.10	56.60	64.52	71.54
CH <sub>4</sub> (% mole fraction)	1.34	0.84	1.07	0.86	1.01	1.29
CO (% mole fraction)	9.97	10.94	10.59	10.14	10.94	5.80

The fluctuation indicated in fig. 3 is a typical showcase of calculation alternating between continuous and dispersed phases. The numerical simulation results are contrasted with experimental data to verify of the present created model. Comparison of the anticipated dry product gas compositions with the experimental data of Chejne and Hernandez [9] is demonstrated in fig. 4.

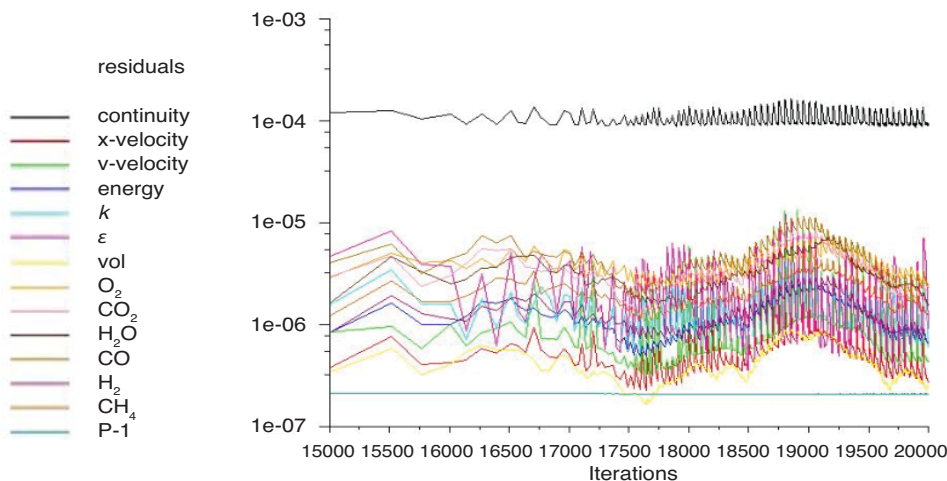


**Figure 3. Typical variable residuals during calculation**  
 (for color image see journal web site)

The mole fractions of gas composition at the gasifier outlet are calculated on the outlet area averaged basis. The outcome demonstrates a decent agreement of these computed gas phase components with experiments. It might be seen that the minimum relative error of calculation to experiment is about 1% and the maximum error is less than 25%. This infers that the current numerical simulation is reasonable and the validity of the current model is verified. In any case, there are slight overestimations for the CO<sub>2</sub> and H<sub>2</sub> and slight underestimation for the CO. This has additionally been seen in the 2-D simulations of a coal gasifier in the same fluidized bed numerical study by Yu *et al.* [21].

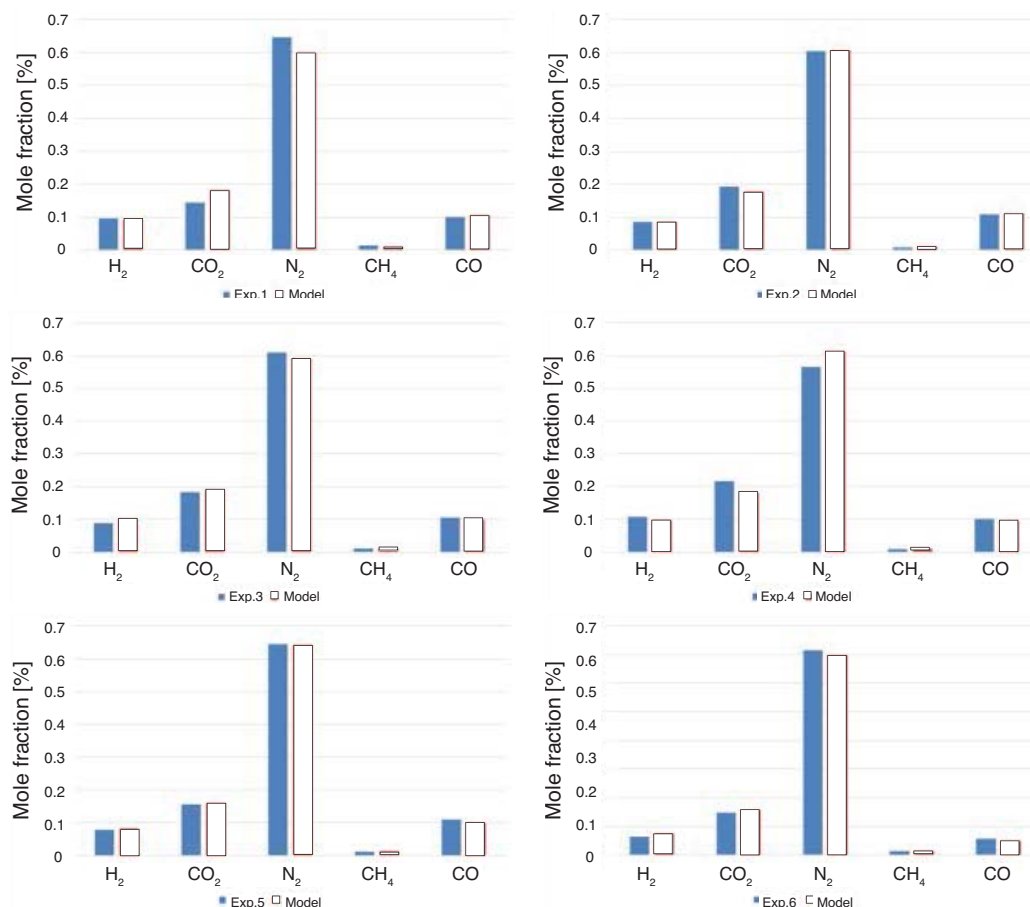
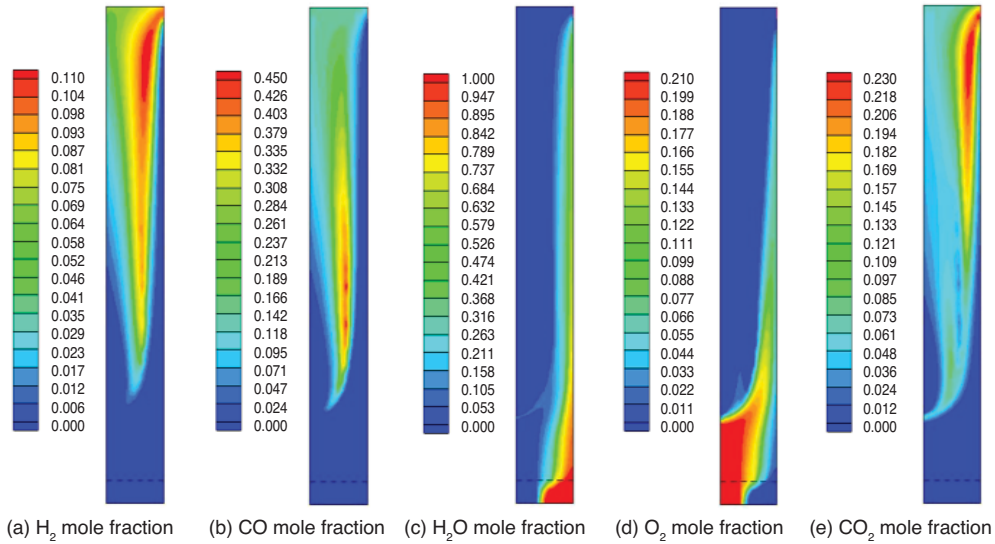


Figure 4. Comparisons between predictions and experimental data in different cases

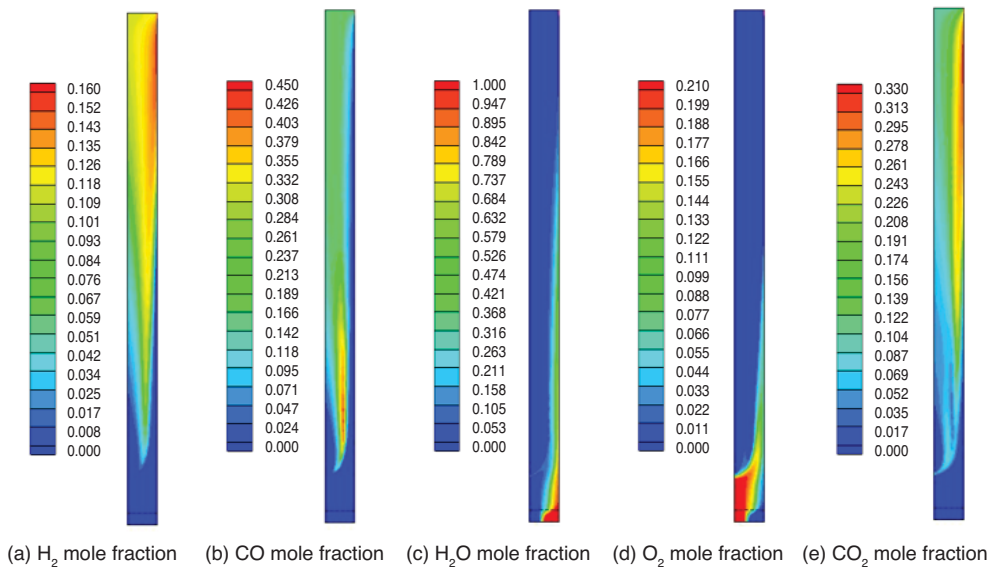
Besides, fig. 5 shows mole fraction distributions (H<sub>2</sub>, CO, H<sub>2</sub>O, O<sub>2</sub>, and CO<sub>2</sub>) in the reactor which has 2 m height. As shown in this figure, the mole fraction of CO<sub>2</sub> is lower due to the existence of a large number of C(s) at the bottom of the gasifier. The mole fraction of CO<sub>2</sub> increases along the height of the gasifier with the decrease of C(s) and volatile combustion. The mole fraction of CO has got the highest value at the coal particle entrance section, the mole fraction of CO decreases along the height of the gasifier while the mole fraction of H<sub>2</sub> increases due to the equilibrium of water-gas shift reaction (R9).

## Result and discussion

After verifying numerical model, the reactor height effect on CO and H<sub>2</sub> mole fractions at the outlet of the gasifier is investigated. Therefore, twelve different reactor heights (1.5, 2, 2.5, 3, 4, 5, 6, 7, 8, 9, 10, and 11 meters) are studied. While examining the reactor height effect on CO and H<sub>2</sub> mole fractions, all the boundary and operating conditions are taken the same as the Exp. 1 of Chejne and Hernandez [9]. Under different reactor heights, mole fraction distributions of CO and H<sub>2</sub> in the reactor are modeled but only one of them is shown in this study for preventing complexities.

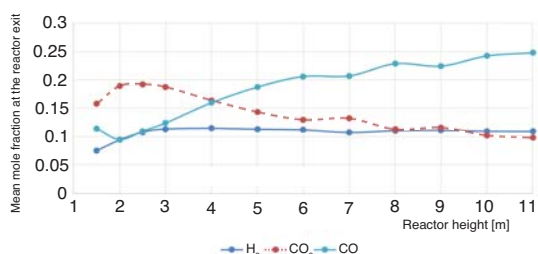


**Figure 5. Mole fraction distributions of H<sub>2</sub>, CO, CO<sub>2</sub>, O<sub>2</sub>, and H<sub>2</sub>O at 2 m reactor height**  
 (for color image see journal web site)



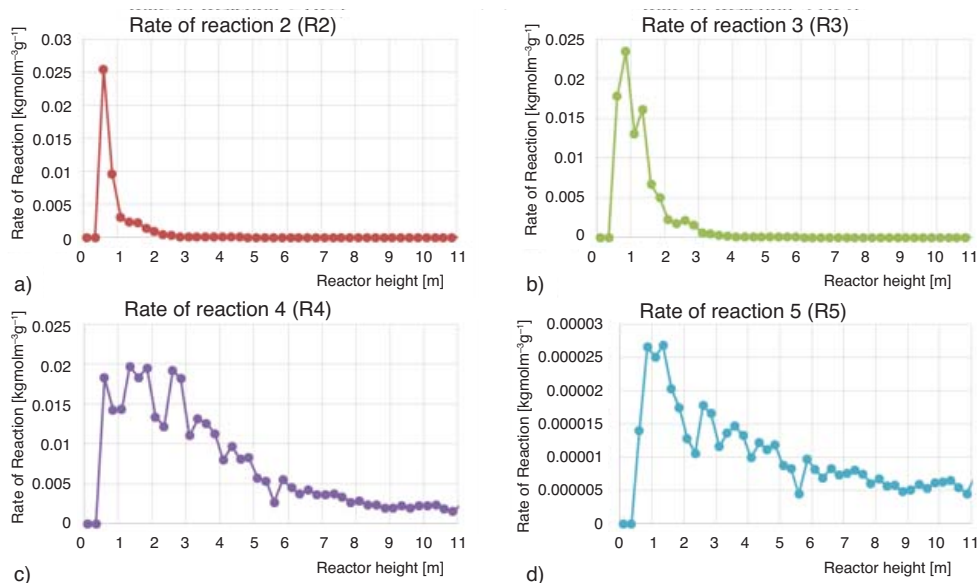
**Figure 6. Mole fraction distributions of H<sub>2</sub>, CO, CO<sub>2</sub>, O<sub>2</sub>, and H<sub>2</sub>O at 4 m reactor height**  
 (for color image see journal web site)

Figure 6 demonstrates CO, H<sub>2</sub>, CO<sub>2</sub>, O<sub>2</sub>, and H<sub>2</sub>O mole fractions in the reactor which has 4 m height. It can be seen from the figure that the general trend of each composition profile is consistent. Close to the coal inlet level of the reactor, the CO concentration is higher because of the presence of a large number of carbon particle and devolatilization. Oxygen and steam are expectedly tailed away near to the feeder. Figure 7 illustrates the reactor height effect on the CO, H<sub>2</sub>, and CO<sub>2</sub> mean mole fractions at the exit of the reactor.



**Figure 7.** Reactor height effect on the H<sub>2</sub>, CO<sub>2</sub>, and CO mean mole fractions at the exit

Mean mole fraction of H<sub>2</sub> is nearly stable after the third meter of the reactor height. Besides this, mean mole fraction of CO is increasing along the height of the reactor. The increasing rate of CO mean mole fraction is very small after 10 meters reactor height. The reactor height effect can be much clearer by showing all reaction rates along the reactor height. Figures 8 and 9 show, respectively, the heterogeneous and homogeneous reaction rates changing along the height of the reactor.



**Figure 8.** Heterogeneous reaction rates changing along the height of the reactor

As shown in these figures, the R6, R7, and R8 reactions are stopped because of the lack of O<sub>2</sub> and H<sub>2</sub>O and their reaction rates are nearly zero after the second meters. The main reason is the fact that the O<sub>2</sub> mean mole fraction is less than 0.005 and also H<sub>2</sub>O mean mole fraction is less than 0.09 after the second meters of the reactor, as shown in the fig. 10.

Water gas shift reaction (R9) rate is almost zero after the 6 meters of the reactor height due to the reactor temperature which is below 1000 K, as shown in fig. 11.

Arrhenius kinetic rate constant,  $k$ , is shown in fig. 12 for water gas shift reaction (R9). As shown in this figure the Arrhenius kinetic rate is very small below 1000 K. Reaction 10 (backward water gas shift reaction) is a very slow reaction because of its rate constant that is shown in tab. 1. Reactions 2 and 3 vanish after the third meters of the reactor height due to the lack of O<sub>2</sub> and H<sub>2</sub>O in the medium. Reaction 4 is the critical reaction because it is very effective to increase the CO mean mole fraction along the reactor height especially above the second meters. Figure 7 illustrates that CO mean mole fraction increases as CO<sub>2</sub> mean mole fraction decreases. The main reason is that reaction 4 (R4) is still active as seen in fig. 8c. The mean mole fraction of CO<sub>2</sub> peaks with temperature and then decreases due to mainly the reaction with carbon (R4).

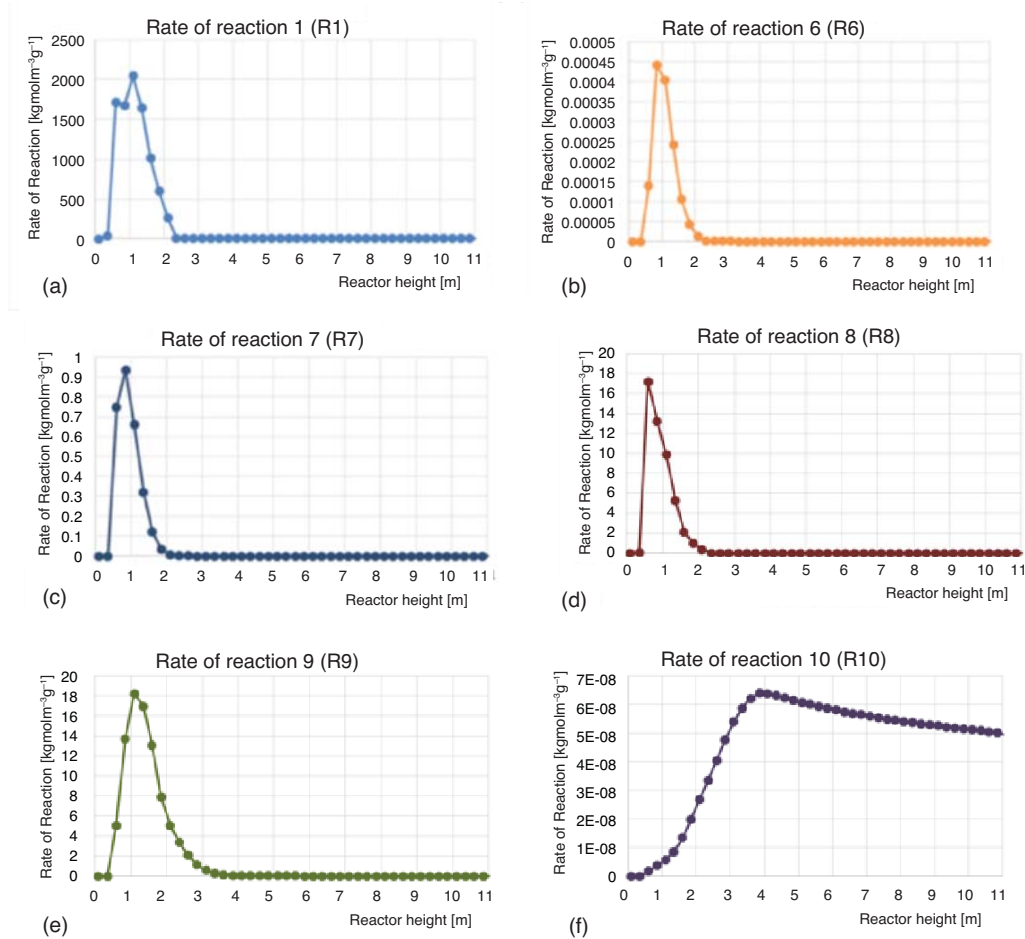


Figure 9. Homogeneous reaction rates changing along the height of the reactor

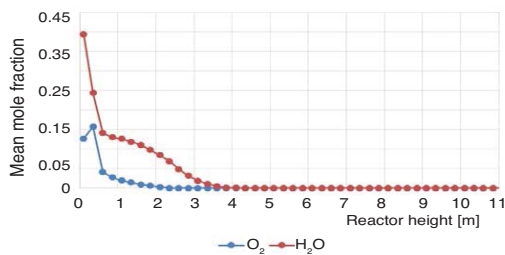


Figure 10. Mean mole fractions of O<sub>2</sub> and H<sub>2</sub>O according to the reactor height

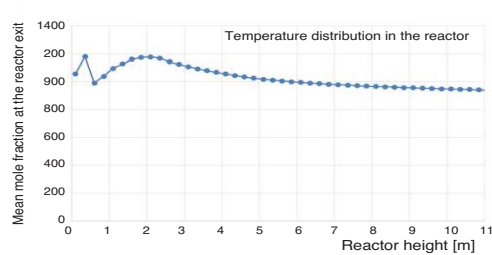
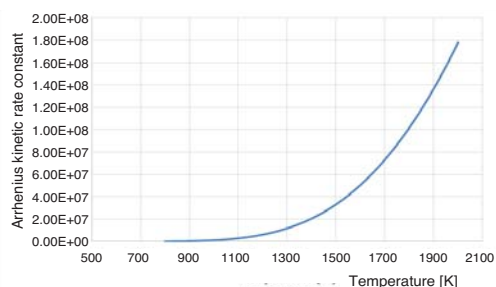


Figure 11. Changing of the reactor averaged temperature by the reactor height

However one should be careful to interpret the graphs because these are relative concentrations which may show a descending character when other gases are being produced. But as seen in fig. 7, the H<sub>2</sub> mean mole fraction is nearly stable.



**Figure 12. Arrhenius kinetic rate constant changing for water gas shift reaction**

homogeneous reactions were used to model gasification process. The effect of reactor height on CO and H<sub>2</sub> mole fraction at the exit of the reactor was investigated. The reactor diameter is 0.22 m. Twelve different (1.5, 2, 2.5, 3, 4, 5, 6, 7, 8, 9, 10, and 11 meters) reactor heights were modeled. Temperature and species distributions were obtained in the reactor. The gas phase was modeled with standard  $k$ - $\epsilon$  turbulence model on Eulerian grid and particle phase was represented by discrete numerical particles. The energy balance equations were used to calculate the thermal conduction within the phase, the heat exchange between gas and solid phases and viscous dissipation. The P-1 radiation model was used in modeling. Segregated solution method was employed in solving the governing equations. Segregated solution method means that governing equations of continuity, momentum, energy, and species transport are solved sequentially. The simulation was steady-state and was used pressure-based solver, which employed an implicit pressure-correction scheme and decoupled the momentum and energy equations. The SIMPLE algorithm was used to couple the velocity and pressure.

The effect of reactor height on the reactor temperature, mean mole fraction of species along the reactor and at the exit of the reactor was investigated. The homogeneous and heterogeneous reaction rates were also obtained. Besides, the calculated exit gas mole fraction values were compared with experimental data in the literature for the 2 meter reactor height situation. It was found that the simulations were in a good fit to the experimental data.

## Nomenclature

$A$	– empirical constant, [units vary]	$R$	– gas constant, [Jmol <sup>-1</sup> K <sup>-1</sup> ]
$\alpha$	– absorption coefficient, [m <sup>-1</sup> ]	$S_f$	– source term due to exchange of momentum, [Nm <sup>-3</sup> ]
$B$	– empirical constant, [units vary]	$S_h$	– source term due to exchange of energy, [Wm <sup>-3</sup> ]
$C$	– linear anisotropic phase function coefficient, [–]	$S_m$	– source term due to exchange of mass, [kgm <sup>-3</sup> s <sup>-1</sup> ]
$C_j$	– molar concentration, [–]	$T$	– temperature, [K]
$C_p$	– heat capacity at constant pressure, [Jkg <sup>-1</sup> K <sup>-1</sup> ]	$u$	– velocity, [ms <sup>-1</sup> ]
$D_t$	– turbulent diffusion coefficient, [m <sup>2</sup> s <sup>-1</sup> ]	$\nu_{i,r}$	– stoichiometric coefficient, [–]
$d$	– diameter of a coal particle, [m]	$Y$	– mass fraction, [–]
$E$	– activation energy, [Jkmol <sup>-1</sup> ]		
$G$	– incident radiation, [Wm <sup>-2</sup> ]		
$g$	– gravitational acceleration, [ms <sup>-2</sup> ]		
$k$	– turbulence kinetic energy, [m <sup>2</sup> s <sup>-2</sup> ]		
$k_{f,r}$	– forward kinetic reaction rate, [units vary]		
$M_w$	– molecular weight, [kgkmole <sup>-1</sup> ]		
$P$	– pressure, [atm]		
$q_r$	– radiation heat flux, [Wm <sup>-2</sup> ]		
		<b>Greek symbols</b>	
		$\epsilon$	– turbulence dissipation rate, [m <sup>2</sup> s <sup>-3</sup> ]
		$\eta$	– rate exponent, [–]
		$\lambda$	– heat conductivity, [Wm <sup>-1</sup> K <sup>-1</sup> ]
		$\lambda_t$	– turbulent heat conductivity, [Wm <sup>-1</sup> K <sup>-1</sup> ]
		$\mu$	– dynamic viscosity, [kgm <sup>-1</sup> s <sup>-1</sup> ]

It means that the mean mole fraction of CO<sub>2</sub> decreases and as a result the mean mole fraction of CO increases. It shows that reaction 4 is very effective for increasing CO mean mole fraction however this effect starts to decrease after the tenth meter height of reactor (figs. 7 and 8c).

## Conclusions

The E-L 2-D numerical models which coupled gas-solid flow with chemical reaction were developed to simulate coal gasification in fluidized bed. Four heterogeneous and six ho-

$\mu_t$	– turbulence viscosity, [ $\text{kgm}^{-1}\text{s}^{-1}$ ]	<i>Subscripts</i>
$\rho$	– density, [ $\text{kgm}^{-3}$ ]	$i, j, k$ – index notation
$\sigma$	– Stefan-Boltzmann constant, [ $\text{Wm}^{-2}\text{K}^{-4}$ ]	$P$ – product
$\sigma_s$	– scattering coefficient, [ $\text{m}^{-1}$ ]	$p$ – particle
$\tau$	– stress tensor, [ $\text{kgm}^{-1}\text{s}^{-2}$ ]	$R$ – reactant
$\Phi$	– viscous dissipation, [ $\text{Jm}^{-3}\text{s}^{-1}$ ]	$t$ – turbulent
		$w$ – wall

## References

- [1] Gomez-Barea, A., Leckner, B., Modeling of Biomass Gasification in Fluidized Bed, *Progress in Energy and Combustion Science*, 36 (2010), 4, pp. 444-509
- [2] Gidaspow, D., *Multiphase Flow and Fluidization: Continuum and Kinetic Theory Description*, Academic Press, San Diego, Cal., USA, 1994
- [3] Wachem, B. V., et al., Eulerian Simulations of Bubbling Behavior in Gas-Solid Fluidised Beds, *Computer & Chemical Engineering*, 22 (1998), Sept., pp. 299-306
- [4] Benyahia, S., et al., Simulation of Particles and Gas Flow Behavior in the Riser Section of a Circulating Fluidized Bed Using the Kinetic Theory Approach for the Particulate Phase, *Powder Technology*, 112 (2000), 1-2, pp. 24-33
- [5] Zhong, W., et al., Flow Behaviors of a Large Spout-Fluid Bed at High Pressure and Temperature by 3D Simulation with Kinetic Theory of Granular Flow, *Powder Technology*, 175 (2007), 2, pp. 90-103
- [6] Wang, X., et al., Three-Dimensional Simulation of Fluidized Bed Coal Gasification, *Chemical Engineering and Processing*, 48 (2009), 2, pp. 695-705
- [7] Tsuji, Y., et al., Discrete Particle Simulation of Two Dimensional Fluidized Bed, *Powder Technology*, 77 (1993), 1, pp. 79-87
- [8] Grabner, M., et al., Numerical Simulation of Coal Gasification at Circulating Fluidised Bed Conditions, *Fuel Processing Technology*, 88 (2007), 10, pp. 948-958
- [9] Chejne, F., Hernandez, J. P., Modelling and Simulation of Coal Gasification Process in Fluidised Bed, *Fuel*, 81 (2002), 13, pp. 1687-1702
- [10] Andrews, M., O'Rourke, P., The Multiple Particle-in-Cell (MP-PIC) Method for Dense Particle Flow, *International Journal Multiphase Flow*, 22 (1996), Apr., pp. 379-402
- [11] Hassan, P., Warn-Gyu, P., Numerical Investigation on Cooling Performance of Ranque-Hilsch Vortex Tube, *Thermal Science*, 18 (1972), 4, pp. 1173-1189
- [12] Tomeczek, J., *Coal Combustion*, Krieger Publishing Company, Malabar, Fla., USA, 1994
- [13] \*\*\*, FLUENT Inc., FLUENT 6.3.26 User Guide, Fluent Inc., Lebanon, N. H., USA, 03766, 2005
- [14] Silaen, A., Wang, T., Effect of Turbulence and Devolatilization Models on Gasification Simulation, *International Journal Heat Mass Transfer*, 53 (2010), 9-10, pp. 2074-2091
- [15] Kobayashi, H., et al., Coal Devolatilization at High Temperatures, *Proceedings*, The Combustion Institute, Boston, Mass, USA, 1977, Vol. 1, pp. 411-425
- [16] Magnussen, B., Hjertager, B., On Mathematical Models of Turbulent Combustion with Special Emphasis on Soot Formation and Combustion, *Proceedings*, The Combustion Institute, Boston, Mass, USA, 1977, Vol. 1, pp. 719-729
- [17] Jones, W., Lindstedt, R., Global Reaction Schemes for Hydrocarbon Combustion, *Combustion and Flame*, 73 (1998), 3, pp. 233-249
- [18] Westbrook, C., Dryer, F., Simplified Reaction Mechanism for the Oxidation of Hydrocarbon in Flames, *Combustion Science and Technology*, 27 (1981), 1-2, pp. 31-43
- [19] Chen, C., et al., Numerical Simulation of Entrained Flow Coal Gasifiers, *Chemical Engineering Science*, 55 (2000), 18, pp. 3861-3883
- [20] Chen, H., Integrated Analyses of Biomass Gasification in Fluidized Beds, Ph. D. thesis, The University of Western Ontario, London, On., Canada, 2007
- [21] Yu, L., et al., Numerical Simulation of the Bubbling Fluidized Bed Coal Gasification by the Kinetic Theory of Granular Flow (KTGF), *Fuel*, 86 (2007), 5-6, pp. 722-734